Highlights of ATLAS Top Quark Physics Results

Davide Malito on Behalf of the ATLAS Collaboration

Abstract

The large amount of top- and antitop-quarks produced at the Large Hadron Collider (LHC) and collected by the ATLAS detector allows to measure the properties of the top quark with unprecedented precision. The study of such properties plays a crucial role in the ATLAS scientific programme, allowing to measure Standard Model parameters with high precision, observe new and rare processes involving the top quark and test and set limits to beyond the standard Model Theories.

Keywords: ATLAS, LHC, top quark
DOI: 10.31526/BSM-2023.5

1. INTRODUCTION

The top quark is the heaviest known elementary particle and due to its large mass it decays before hadronising, allowing the direct measurement of its properties. The top quark decays into a b quark and a W boson, which can decay either into a lepton and a neutrino or into quarks, allowing to categorize events where a top quark or a top-quark pair are produced into leptonic, hadronic or semileptonic channels. The precise measurement of its properties allows to perform stringent tests of the Standard Model (SM), as well as to search for new physics beyond the Standard Model (BSM) since it is predicted by several models that the production rate of processes involving the top quark can be changed in the presence of new physics. Furthermore, the top quark contributes as a background event in several processes. Therefore, top-quark properties, e.g., mass, spin or couplings, and production modes via strong and electroweak interaction need to be measured and known with high precision. The ATLAS experiment [1] presents some of the recent highlights of top-quark measurements, including inclusive and differential measurements [2, 3, 4, 5, 6, 7, 8, 9], observation of rare production modes [10, 11] and top-quark properties measurements [12, 13, 14]. The presented results are just a subset of the recent highlights of the ATLAS top-quark physics results.

2. HIGHLIGHTS OF ATLAS TOP PHYSICS RESULTS

2.1. *Measurement of the $t\bar{t}$ Cross-Section and Its Ratio to the Z Production Cross-Section Using pp Collisions at $\sqrt{s} = 13.6$ TeV with the ATLAS Detector*

The measurement of the $t\bar{t}$ cross-section and its ratio to the Z production cross-section at $\sqrt{s} = 13.6$ TeV is the first measurement performed using Run3 data [2]. The data used in this analysis corresponds to an integrated luminosity of 29 fb^{-1}. This analysis uses $t\bar{t}$ events in the dilepton $e\mu$ channel, while the Z-boson decays to a pair of electrons or muons. Three channels are thus defined using electrons and muons of opposite electric charge: ee, $\mu\mu$ and $e\mu$. The analysis uses a method where the number of events with one and two b-tagged jets are counted separately, allowing the $t\bar{t}$ cross-section to be extracted together with the efficiency to identify a b-tagged jet. Opposite sign electron-muon pairs are selected and the number of events that have one b-tagged jet and two b-tagged jets (N_2) are counted, where N_1 and N_2 are defined as

$$\begin{aligned} N_1 &= L\sigma_{t\bar{t}}\epsilon_{e\mu}2\epsilon_b\left(1 - C_b\epsilon_b\right) + N_1^{\text{bkg}}, \\ N_2 &= L\sigma_{t\bar{t}}\epsilon_{e\mu}C_b\epsilon_b^2 + N_2^{\text{bkg}}, \end{aligned} \tag{1}$$

where L is the integrated luminosity, $\sigma_{t\bar{t}}$ is the measured $t\bar{t}$ cross-section, ϵ_b is the combined probability to reconstruct and b-tag a b-jet after the selection, and $\epsilon_{e\mu}$ is the efficiency for a $t\bar{t}$ event to pass the opposite sign $e\mu$ selection, C_b represents the probability to reconstruct and tag both b-jets, may deviate slightly from unity due to kinematic correlations of the b-jets produced in a $t\bar{t}$ event and is estimated from simulation. Similarly, the same-flavor channels (ee, $\mu\mu$) are used to extract the Z production cross-section. A profile-likelihood fit is employed to simultaneously extract the $t\bar{t}$ cross-section, the Z boson cross-section and the b-tagging efficiency in all three channels. A second profile-likelihood fit is used to measure the ratio of the $t\bar{t}$ cross-section and the Z boson cross-section.

Talk presented at the Beyond the Standard Model conference (BSM 2023), 06–09 November 2023.

The measured cross-sections and their ratio are

$$\begin{aligned} \sigma_{t\bar{t}} &= 850 \pm 3(\text{stat.}) \pm 18(\text{syst.}) \pm 20(\text{lumi.})\,\text{pb}, \\ \sigma^{\text{fid.}}_{Z\to\ell\ell} &= 744 \pm 11(\text{stat.}+\text{syst.}) \pm 16(\text{lumi.})\,\text{pb}, \\ R_{t\bar{t}/Z} &= 1.145 \pm 0.003(\text{stat.}) \pm 0.021(\text{syst.}) \pm 0.002(\text{lumi.}) \end{aligned} \tag{2}$$

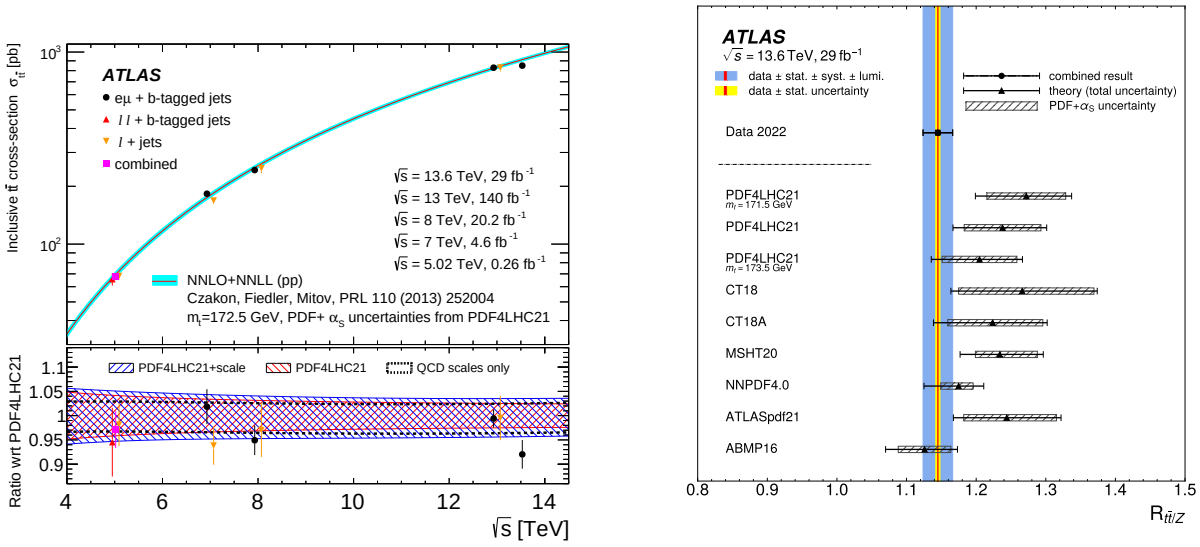

(a) (b)

FIGURE 1: (a) Comparison of the measured $t\bar{t}$ cross-sections at various center-of-mass energies and the theory predictions using the PDF4LHC21 PDF set. The bottom panel shows the ratio of the measured values and three predictions that either contain only the uncertainties originating from the QCD scale variations (black), only the variations in the PDF uncertainties (red) or the total uncertainty in the prediction (blue). (b) Ratio of the $t\bar{t}$ to the Z-boson cross-section compared to the predictions for several sets of parton distribution functions. For the PDF4LHC21 PDF set, predictions for different assumptions about the top-quark mass are also displayed [2].

As illustrated in Figure 1, the measured $t\bar{t}$ cross-section is very close, but not in agreement with the SM prediction using the PDF4LHC21 PDF set. The largest uncertainty for the $t\bar{t}$ cross-section is the theory uncertainty on the modelling of the signal parton shower.

2.2. *Inclusive and Differential Cross-Sections for Single-Lepton and Dilepton $t\bar{t}$ Production Measured in $\sqrt{s} = 13\,TeV$ pp Collisions with the ATLAS Detector*

Top-quark pairs are largely produced at the LHC, allowing to measure the cross-section with unprecedented precision. Furthermore the measurement of differential cross-sections are particularly interesting because they allow to further test the SM and to highlight the differences with Monte Carlo (MC) predictions. The cross-sections are measured both in the dilepton channel [4] and in the semileptonic channel [3]. The lepton measurement focuses on the $e\mu$ channel and uses a similar method as the Run3 analysis (Section 2.1) to extract the cross-section. The measured cross-section in the fiducial particle-level phase space is

$$\sigma^{\text{fid}}_{t\bar{t}} = 10.53 \pm 0.02(\text{stat.}) \pm 0.13(\text{syst.}) \pm 0.10(\text{lumi.}) \pm 0.02(\text{beam})\,\text{pb}, \tag{3}$$

that, extrapolated to the full phase space, leads to the most precise $t\bar{t}$ cross-section to date

$$\sigma_{t\bar{t}} = 829 \pm 1(\text{stat.}) \pm 13(\text{syst.}) \pm 8(\text{lumi.}) \pm 2(\text{beam})\,\text{pb}. \tag{4}$$

The semileptonic one uses an Iterative Bayesian Unfolding to measure the differential cross-sections as a function of jet kinematic observables. An example of differential distribution for both the analyses is presented in Figure 2.

2.3. *Observation of Four-Top-Quark Production in the Multilepton Final State with the ATLAS Detector*

The associated production of four top-quarks is a very rare SM process, which cross-section is enhanced in several BSM theories. Additionally, the $t\bar{t}t\bar{t}$ cross-section is sensitive to the strength of the top-quark Yukawa coupling, and its charge conjugation and

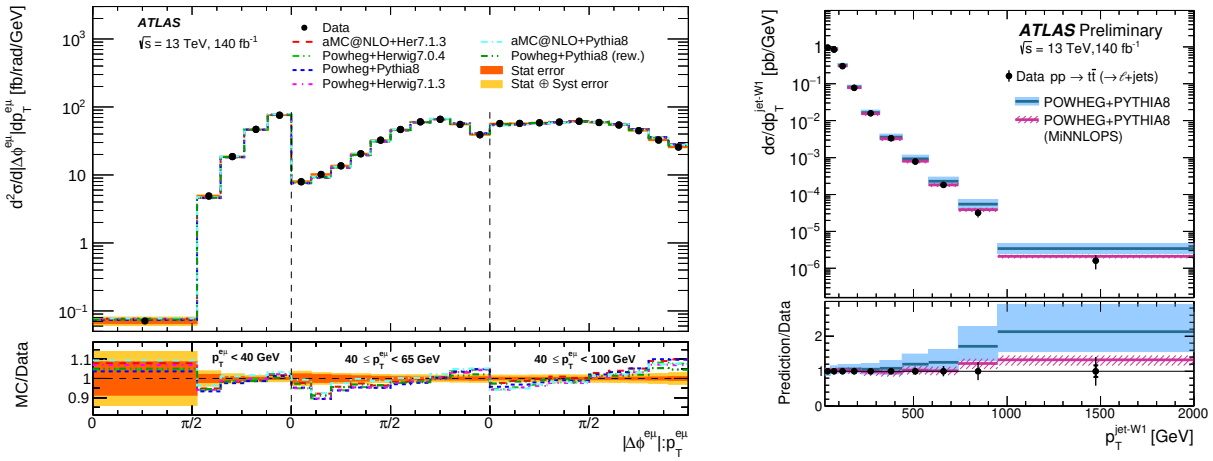

(a) (b)

FIGURE 2: (a) Absolute double-differential cross-sections as a function of $|\Delta\phi e\mu|$ in bins of $p_T^{e\mu}$ with statistical (orange) and statistical plus systematic uncertainties (yellow). The data points are placed at the center of each bin. The results are compared with the predictions from different Monte Carlo generators. The lower panel shows the ratios of the predictions to data, with the bands indicating the statistical and systematic uncertainties [4]. (b) The measured normalized differential cross sections for $t\bar{t}$ production as functions of $p_T^{\text{jet}-\text{W}^1}$. The NLO QCD predictions from Pwg+Py8 (blue lines) and the NNLO QCD predictions from Pwg+Py8 MiNNLOPS (purple lines) are also shown. The lower part of the figures show the ratio of the predicted and the measured cross sections [3].

parity properties. The measurement [10] uses a maximum likelihood fit approach to extract the cross-section $\sigma_{t\bar{t}t\bar{t}}$ from the output of a Graph Neural Network (GNN) in several signal and control regions. Furthermore limits are set on Effective Field Theory (EFT) operators, $\sigma_{t\bar{t}t}$ and the oblique Higgs parameter. The measured cross-section is

$$\sigma_{t\bar{t}t\bar{t}} = 22.5^{+4.7}_{-4.3}(\text{stat})^{+4.6}_{-3.4}(\text{syst})\,\text{fb} = 22.5^{+6.6}_{-5.5}\,\text{fb} \tag{5}$$

and is found to be 6.1σ away from the null hypothesis. The limit on the top-Yukawa coupling strength modifier is found to be $|\kappa_t| < 1.8$, while the Higgs oblique parameter limits are $\hat{H} < 0.20\ (0.12)$, compatible with the SM. The results for the $t\bar{t}t$ cross-section versus the $t\bar{t}t\bar{t}$ cross-section are shown in Figure 3.

2.4. *Observation of $t\bar{t}$ Production in Lepton+Jets and Dilepton Channels in p + Pb Collisions at $\sqrt{s_{NN}} = 8.16$ TeV with the ATLAS Detector*

The measurement of the production of top pairs in heavy-ion collisions [11] provides novel probes of nuclear modifications to parton distribution functions (nPDF) in previously poorly constrained phase spaces. Moreover top quarks are expected to provide unique information on the properties of the strongly interacting quark-gluon plasma. The measurement uses $165\,\text{nb}^{-1}$ of pPb collisions data collected by the ATLAS detector during 2016 at a nucleus-nucleus center-of-mass energy of $\sqrt{s_{NN}} = 8.16\,\text{GeV}$. To measure the cross-section A profile-likelihood fit is used to extract the cross section from the distribution of the scalar sum of the lepton and the jets transverse momentum (H_T^{ljet}). The measured cross-section is found to be

$$\sigma_{t\bar{t}} = 57.9 \pm 2.0(\text{stat})^{+4.9}_{-4.5}(\text{syst})\,\text{nb}. \tag{6}$$

2.5. *Measurement of t-Channel Single-Top-Quark Production in pp Collisions at $\sqrt{s} = 5.02$ TeV and at $\sqrt{s} = 13$ TeV with the ATLAS Detector*

The top-quark can be produced either as a pair or singly in weak charged-current interactions. The dominant single-top-quark production process at the LHC is characterized by the t-channel exchange of a virtual W boson. Since the valence u-quark density of the proton is about twice as high as the valence d-quark density, the production cross-section of single top quarks is expected to be higher than the cross-section of top-antiquark production. The study of the production of single can provide a very interesting testing ground for SM predictions. The cross-section is measured using $255\,\text{pb}^{-1}$ pp collision data at $\sqrt{s} = 5.02\,\text{TeV}$ [6] and by using $140\,\text{fb}^{-1}$ pp collision data at $\sqrt{s} = 13\,\text{TeV}$ [5]. In the $\sqrt{s} = 5.02\,\text{TeV}$ analysis a profile-likelihood fit is used in the top and antitop channels to extract the cross-sections and their ratio (R_t), which are found to be

$$\begin{aligned} \sigma(tq + \bar{t}q) &= 27.1^{+4.4}_{-4.1}\,(\text{stat})^{+4.4}_{-3.7}\,(\text{syst})\,\text{pb}, \\ R_t &= 2.73^{+1.43}_{-0.82}\,(\text{stat})^{+1.01}_{-0.29}\,(\text{syst}). \end{aligned} \tag{7}$$

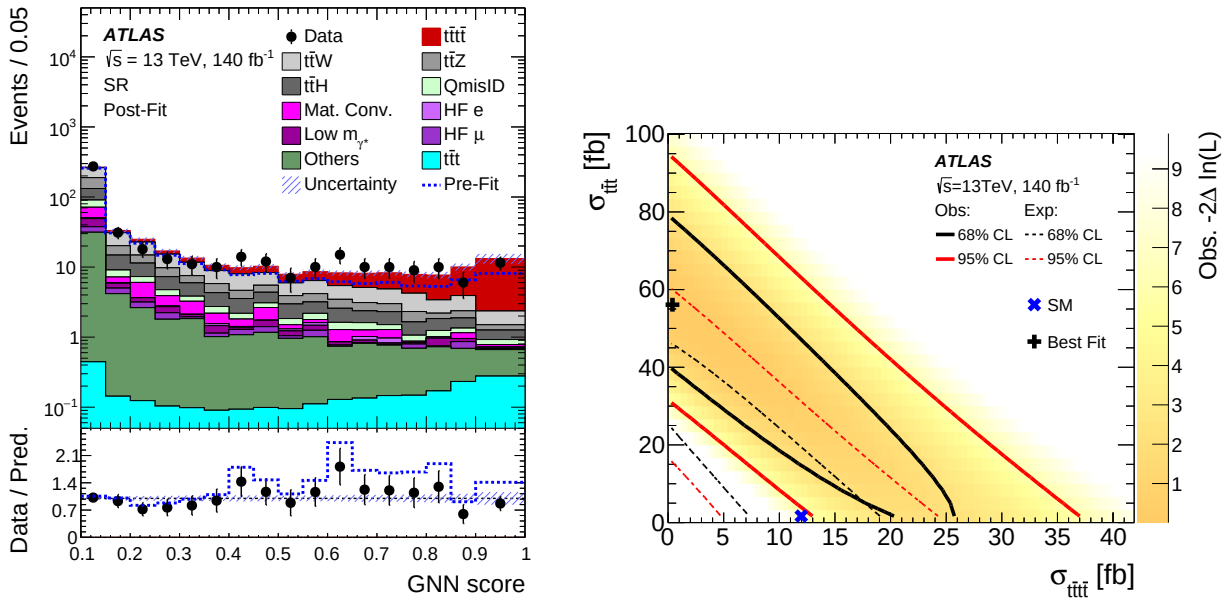

(a) (b)

FIGURE 3: (a) Comparison between data and the predictions after a fit to data for the GNN distribution in the SR. (b) Two-dimensional negative log-likelihood contour for the $t\bar{t}t$ cross-section ($\sigma_{t\bar{t}t}$) versus the $t\bar{t}t\bar{t}$ cross-section ($\sigma_{t\bar{t}t\bar{t}}$) when the normalization of both processes are treated as free parameters in the fit [10].

Additionally, since the t-channel single-top-quark production cross-section depends on $f_{LV}^2 \cdot |V_{tb}^2|$, where f_{LV} is a left-handed form factor that is unity in the SM and V_{tb} is a component of the Cabibbo-Kobayashi-Maskawa (CKM) matrix, the value of $f_{LV} \cdot |V_{tb}|$ has also been measured

$$f_{LV} \cdot |V_{tb}| = 0.94^{+0.11}_{-0.10}. \tag{8}$$

The $\sqrt{s} = 13\,\text{TeV}$ analysis also uses a profile-likelihood approach to measure the cross-sections, their ratio and the CKM matrix element. In addition limits on the $C_{qQ}^{(1,3)}$ EFT operator are set. The measured inclusive cross-section and the ratio of top-antitop production are found to be

$$\begin{aligned} \sigma(tq + \bar{t}q) &= 221 \pm 13\,\text{pb}, \\ R_t &= 1.636^{+0.036}_{-0.034}, \end{aligned} \tag{9}$$

while the CMK matrix element is

$$f_{LV} \cdot |V_{tb}| = 1.016 \pm 0.031. \tag{10}$$

Finally the limits on the EFT operator are found to be

$$-0.25 < C_{qQ}^{(1,3)} < 0.12. \tag{11}$$

A comparison of the measured cross-section and ratio is presented in Figure 4.

2.6. Measurement of Jet Substructure in Boosted $t\bar{t}$ Events with the ATLAS Detector Using 140 fb^{-1} of 13 TeV pp Collisions

The precise study of the substructure of the jets originating from the top quark decay products is an important part of the ATLAS top quark physics programme. It allows tests of the Standard Model SM at both the top-quark mass scale relevant for substructure measurements and the TeV scales relevant for jet production measurements, as well as search for BSM physics, that would show up as deviations of top-quark jet substructure from the SM predictions. Furthermore top-quark jet substructure is employed in the development of sophisticated taggers, used to separate top-quark jets from energetic jets arising from lighter quarks or gluons. This measurements [9] focuses on both semileptonic and all hadronic top-pair events in which the top quarks are produced with a transverse momentum usually above 300 GeV, resulting in particles can be studied as a single, collimated system, called large-R jet. The analysis aims to measure differential cross-sections as a function of observables characterizing the internal structure of the large-R jets. The distributions are unfolded to particle-level using an iterative bayesian unfolding. The measured substructure variables are the N-subjettiness variable τ_3, as well as the ratios $\tau_{32} = \tau_3/\tau_2$, the normalized energy-correlation function ECF2, as well as the associated variables D_2 and C_3, and the Les Houches angularity LHA and the scaled p_T dispersion $p_T^{d,*}$, which are two generalized angularities.

In Figure 5, a double-differential cross section is presented as a function of τ_{23} and jet mass.

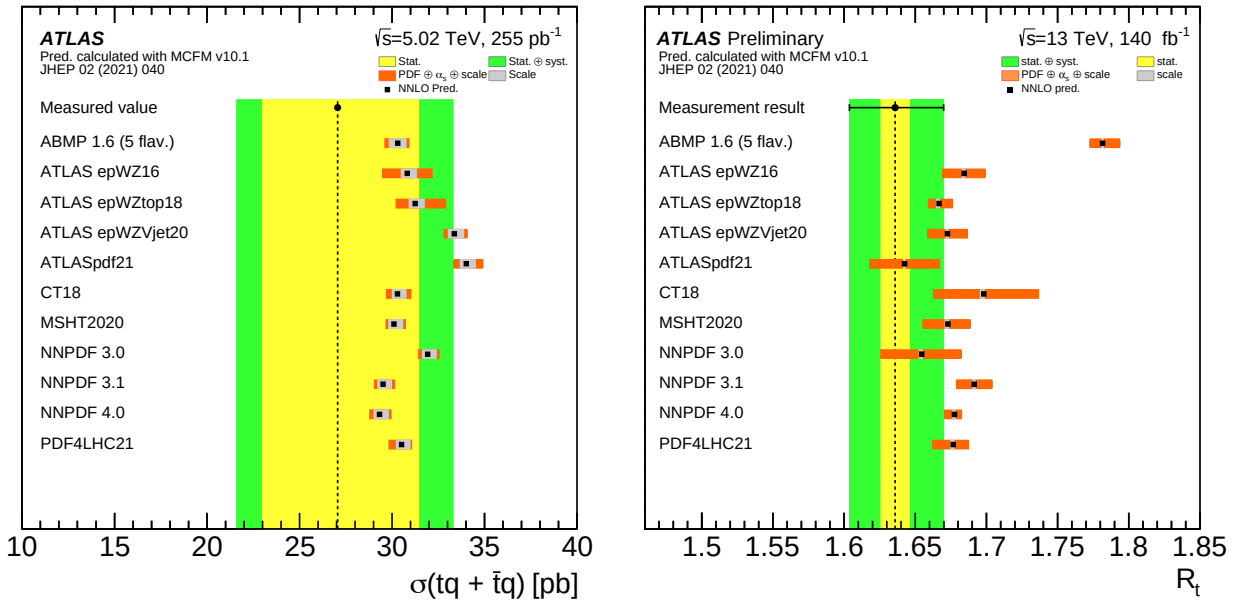

(a) (b)

FIGURE 4: (a) The measured $\sigma(tq + t\bar{q})$ at $\sqrt{s} = 5.02\,\text{TeV}$. The dashed line and the dot show the measured value, the yellow band displays the statistical uncertainty, and the green band displays the total uncertainty on the measurement. For comparison, the predictions of MCFM based on different PDFs are included. The gray (orange) band represents the uncertainty on the predictions [6]. (b) The measured value of R_t. The yellow band represents the statistical uncertainty and the green band the total uncertainty of the measurement. For comparison the NNLO prediction of MCFM based on different PDF sets are also included [5].

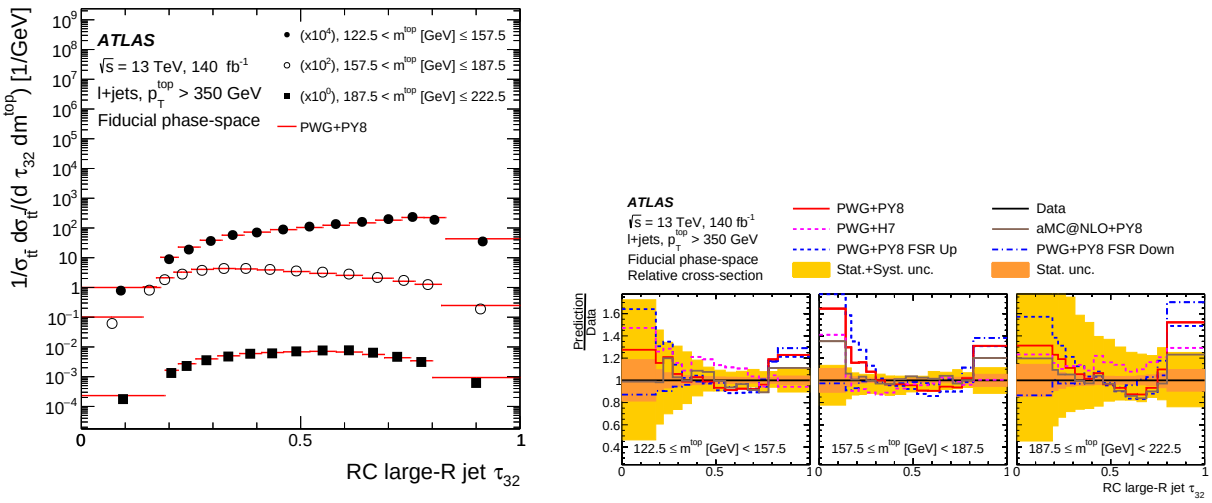

(a) (b)

FIGURE 5: Particle-level differential $t\bar{t}$ production cross-section as a function of τ_{23} and jet mass, for several NLOME+PS predictions of $t\bar{t}$ signal and the data. The events shown here are from the ℓ+jets channel: (a) shows the data and the nominal prediction, while (b) shows the ratios of the predictions to the data. The lighter band represents the total uncertainty of the measured differential cross-section, while the darker band shows the statistical component [9].

2.7. *Search for Flavor-Changing Neutral tqH Interactions with $H \to \gamma\gamma$ in pp Collisions at $\sqrt{s} = 13\,TeV$ Using the ATLAS Detector*

According to the SM, Flavor Changing Neutral Current (FCNC) processes are forbidden at tree level and very much suppressed at the one-loop level and higher orders due to the Glashow-Iliopoulos- Maiani mechanism. Observations of FCNC decays of the top quark, which are extremely rare in the SM would therefore constitute a clear signal of new physics. An example of an FCNC process is the production of a top quark alongside an Higgs boson and another quark. In this measurement [14] a search for FCNC

is performed in the $tqH(\gamma\gamma)$ channel in both the leptonic and hadronic top quark decay channels. Furthermore a combination with previous ATLAS measurements performed in the $b\bar{b}$ and $\tau\tau$ Higgs decay channels is also performed. The branching ratios of a top quark decaying into a lighter quark (c, u) alongside an Higgs boson is measured with a profile-likelihood fit and the measured (expected) upper limits are

$$\begin{aligned} BR(t \to cH) &< 4.3 \times 10^{-4} \ \left(4.7 \times 10^{-4}\right), \\ BR(t \to uH) &< 3.8 \times 10^{-4} \ \left(3.9 \times 10^{-4}\right). \end{aligned} \tag{12}$$

The results of the combination and the comparison with both the results from other FCNC searches and the one from this analysis are shown in Figure 6.

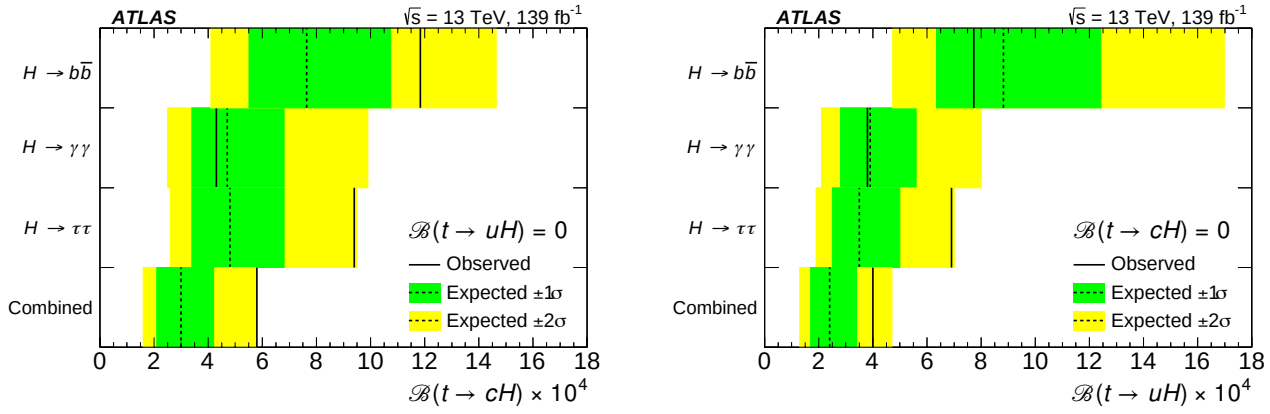

(a) (b)

FIGURE 6: 95% CL upper limits on (a) cal $B(t \to cH)$ assuming cal $B(t \to uH) = 0$ and (b) cal $B(t \to uH)$ assuming cal $B(t \to cH) = 0$ for the individual searches and their combination. The observed limits (solid lines) are compared with the expected (median) limits under the background-only hypothesis (dotted lines). The surrounding shaded bands correspond to the 68% and 95% CL intervals around the expected limits, denoted by $\pm 1\sigma$ and $\pm 2\sigma$, respectively, [14].

2.8. *Measurement of the Total and Differential Cross-Sections of $t\bar{t}W$ and $t\bar{t}Z$ Production in pp Collisions at 13 TeV with the ATLAS Detector*

The production of a $t\bar{t}$ pair in association with a Z or a W are two rare processes of the SM. A precise measurement of their inclusive and differential cross-sections [7, 8] provide a strict test of the SM and can also be used to measure asymmetries, provide inputs for EFT interpretations and can be useful for other measurements where they are one of the main backgrounds. Moreover they are key ingredients in many BSM searches. Both the analyses use a profile-likelihood fit in several signal and control regions in order to extract the production cross-section. Furthermore the $t\bar{t}W$ analysis uses a profile-likelihood unfolding to measure differential distributions.

The measured inclusive cross-sections are

$$\begin{aligned} \sigma(t\bar{t}W) &= 890 \pm 50 \ (\text{stat.}) \pm 70 \ (\text{syst.}) = 890 \pm 80 \ \text{fb}, \\ \sigma(t\bar{t}Z) &= 0.86 \pm 0.04 \ (\text{stat.}) \pm 0.04 \ (\text{syst.}) \ \text{pb}. \end{aligned} \tag{13}$$

The $t\bar{t}W$ analysis also measured the ratio of the production of $t\bar{t}W^+/t\bar{t}W^-(R(t\bar{t}W))$ and the relative charge asymmetry

$$\begin{aligned} R(t\bar{t}W) &= 1.95^{+0.21}_{-0.18} \ (\text{stat.})^{+0.16}_{-0.13} \ (\text{syst.}), \\ A_C^{\text{rel}} &= \frac{\sigma\left(t\bar{t}W^+\right) - \sigma\left(t\bar{t}W^-\right)}{\sigma\left(t\bar{t}W^+\right) + \sigma\left(t\bar{t}W^-\right)} = 0.32 \pm 0.05 \ (\text{stat.}) \pm 0.03 \ (\text{syst.}). \end{aligned} \tag{14}$$

Finally, the results of a differential distribution and the EFT interpretation results can be found in Figure 7.

2.9. *Combination of Measurements of the Top-Quark Mass from Data Collected by the ATLAS and CMS Experiments at $\sqrt{s} = 7$ and 8 TeV*

The mass of the top quark (m_t) is one of the fundamental parameters of the SM. A precise measurement of its value provides a crucial input to fits that probe the consistency of the SM. During Run1 the two multi-purpose LHC detectors, ATLAS and CMS, performed several measurements of the top-quark mass, typically with an uncertainty below 1 GeV, of which the combined results is presented [12]. The measurements are combined using the BLUE method [15], which defines the estimator $m_t = \Sigma_i w^i m_t^i$, for

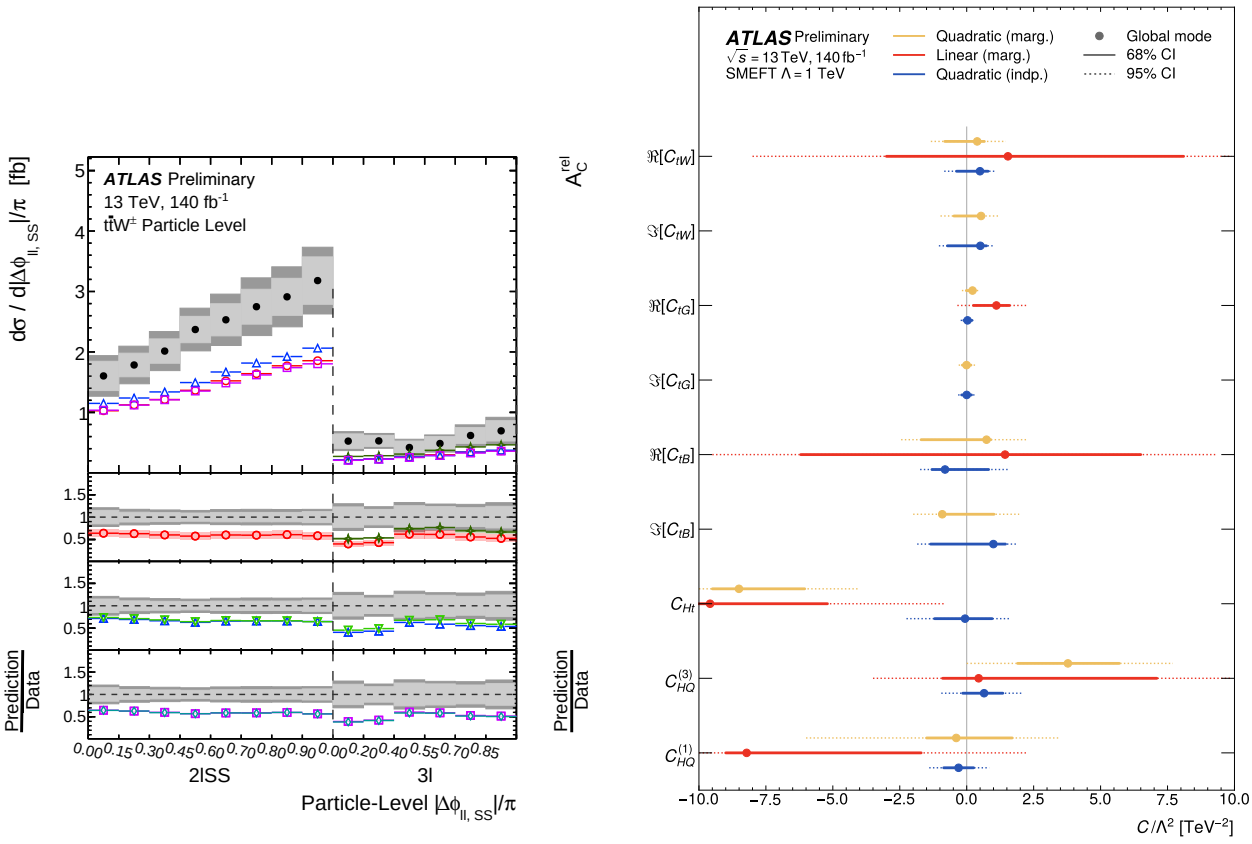

(a) (b)

FIGURE 7: (a) Unfolded results for the absolute differential cross-section and A_C^{rel} measurements as a function of $|\Delta\phi, \text{SS}|/\text{ß}$. The colored markers overlaid upon the cross-section measurements show different theoretical predictions. The breakdown of statistical-only uncertainties are shown in light grey and combined statistical and systematic uncertainties are shown in dark grey [8]. (b) Comparison of the 68% and 95% credible intervals obtained in the top-boson scenario. Also shown are the best-fit values (global mode) for each operator [7].

the set of input measurements m_t^i. The weights w_i are determined by minimizing the uncertainty in m_t, where the covariance between each pair of measurements is the crucial input. The individual measurements are defined to be orthogonal, such that each measurement is statistically uncorrelated with every other measurement. The measurements share similar systematic uncertainties and the assessment of their correlation is central to the combination. As the treatment of systematic uncertainties differs between ATLAS and CMS, for each measurement they are mapped onto 25 categories, and a correlation strength ρ is defined and is assumed to have three values, $\rho = 0.85$ (strongly correlated), $\rho = 0.5$ (partially correlated) and $\rho = 0$ (uncorrelated).

In Figure 8, a summary of the measurements and their combination is presented. The measurements from each experiment have been combined in order to provide an ATLAS and a CMS mass combination which then combined proved the LHC combination. The results of the combinations are

$$\begin{aligned} m_t^{\text{ATLAS}} &= 172.71 \pm 0.25\ (\text{stat.}) \pm 0.41\ (\text{syst.})\ \text{GeV}, \\ m_t^{\text{CMS}} &= 172.52 \pm 0.14\ (\text{stat.}) \pm 0.39\ (\text{syst.})\ \text{GeV}, \\ m_t^{\text{LHC}} &= m_t = 172.52 \pm 0.14\ (\text{stat.}) \pm 0.30\ (\text{syst.})\ \text{GeV}. \end{aligned} \tag{15}$$

2.10. *Observation of Quantum Entanglement in Top-Quark Pair Production Using pp Collisions of $\sqrt{s} = 13$ TeV with the ATLAS Detector*

One of the most important feature of quantum mechanics is the quantum entanglement, which has application in field such as metrology, cryptography, quantum information, and quantum computation. If two particles are entangled, their quantum state cannot be described individually. This measurement [13] aims to demonstrate the quantum entanglement between two top quarks at a never presented before energy scale. In order to do so an entanglement marker, D, is defined as

$$D = \text{tr}[C]/3 = -3 \cdot \langle \cos(\phi) \rangle, \tag{16}$$

where $\langle \cos(\phi) \rangle$ is the average value of the cosine of the angle (dot product) between the charged lepton directions after they have been Lorentz boosted into the $t\bar{t}$ rest frame and then their parent top-quark and antitop-quark's rest frames, which can be measured experimentally in an ensemble data set. The existence of an entangled state is demonstrated if the measurement satisfies $D < -1/3$. Three analysis region were defined: one where entanglement is expected to be found ($340 < m_{t\bar{t}} < 380\,\text{GeV}$) and two validation regions wick are expected to have low or zero entanglement ($380 < m_{t\bar{t}} < 500\,\text{GeV}$, $m_{t\bar{t}} > 500\,\text{GeV}$).

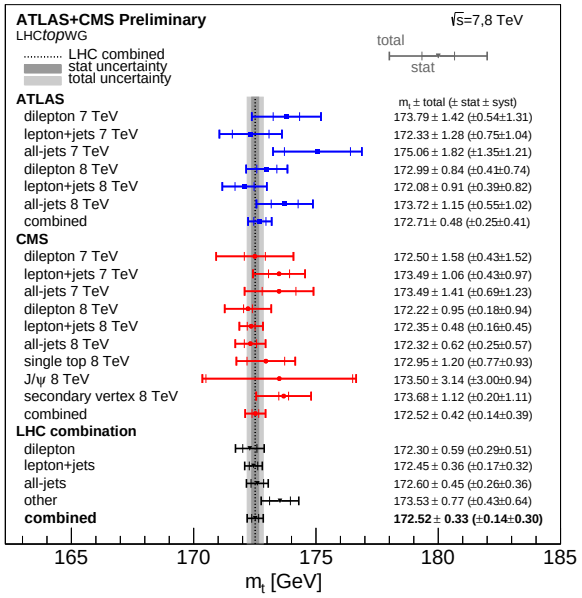

FIGURE 8: Comparison of the individual mt measurements and the result of the overall LHC Run 1 m_t combination. Also shown are the separate combinations of each experiment and the result of the simultaneous combination for the different decay channels, where the "other" category covers the single-top, J/ψ and secondary vertex measurements [12].

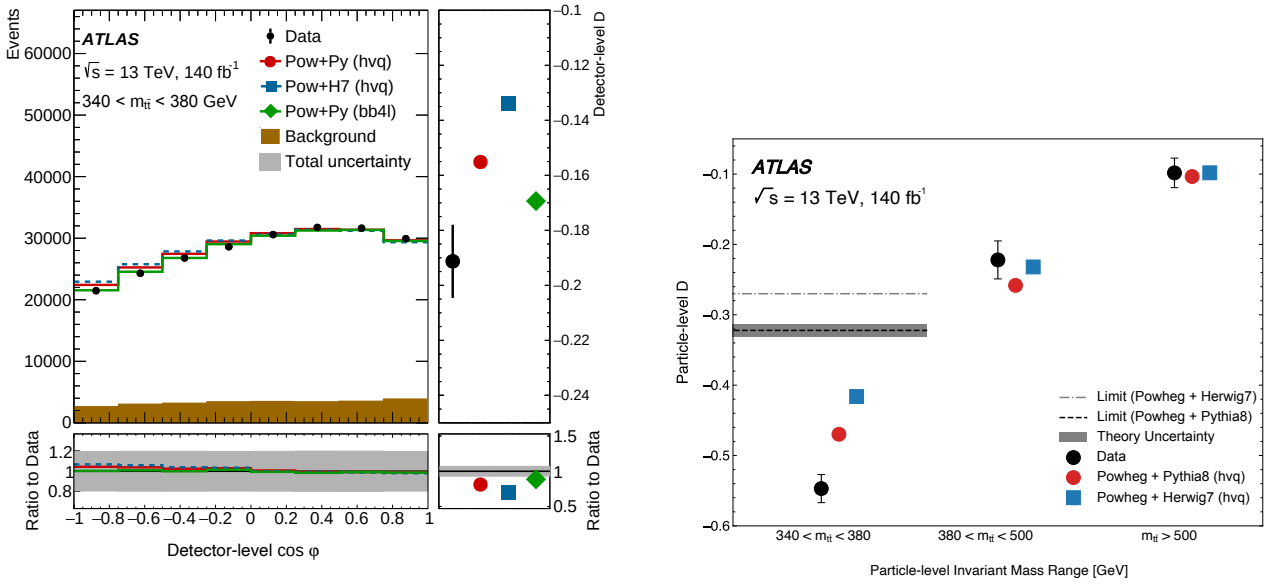

(a) (b)

FIGURE 9: (a) The left panel shows the $\cos\phi$ observable in the signal region at detector level and the right panel shows the entanglement marker D, calculated from the detector-level distributions, from three different MC generators. The uncertainty band shows the uncertainties from all sources added in quadrature. The ratios of the predictions to the data are shown at the bottom of the figure. (b) The particle-level D results in the signal and validation regions compared with various MC models. The entanglement limit shown is a conversion from its parton-level value of $D < -1/3$ to the corresponding value at particle level, and the uncertainties [13].

In order to compare the data with calculations and correct for detector effects the measured values for D are unfolded to a fiducial particle-level volume, while the theoretical predictions are "folded" from parton- to particle-level. Both the folding and unfolding are done using a dedicated calibration curve.

In Figure 9, the value of $\cos\phi$ distribution and detector-level D in the signal region, as well as the unfolded results for the three analysis regions are shown.

References

[1] ATLAS Collaboration. The ATLAS Experiment at the CERN Large Hadron Collider. *JINST*, 3:S08003, 2008. doi: 10.1088/1748-0221/3/08/S08003.

[2] ATLAS Collaboration. Measurement of the $t\bar{t}$ cross section and its ratio to the Z production cross section using pp collisions at $\sqrt{s} = 13.6$ TeV with the ATLAS detector. *arXiv: 2308.09529 [hep-ex]*, 2023.

[3] ATLAS Collaboration. Measurement of differential cross sections in $t\bar{t}$ and $t\bar{t}$+jets production in the lepton+jets decay mode in pp collisions at $\sqrt{s} = 13$ TeV using 140 fb^{-1} of ATLAS data. ATLAS-CONF-2023-068, 2023. URL `https://cds.cern.ch/record/2873524`.

[4] ATLAS Collaboration. Inclusive and differential cross-sections for dilepton $t\bar{t}$ production measured in $\sqrt{s} = 13$ TeV pp collisions with the ATLAS detector. *JHEP*, 07:141, 2023. doi: 10.1007/JHEP07(2023)141.

[5] ATLAS Collaboration. Measurement of t-channel production of single top quarks and antiquarks in pp collisions at 13 TeV using the full ATLAS Run 2 dataset. ATLAS-CONF-2023-026, 2023. URL `https://cds.cern.ch/record/2860644`.

[6] ATLAS Collaboration. Measurement of t-channel single-top-quark production in pp collisions at $\sqrt{s} = 5.02$ TeV with the ATLAS detector. *arXiv: 2310.01518 [hep-ex]*, 2023.

[7] ATLAS Collaboration. Measurement of the total and differential cross-sections of $t\bar{t}W$ production in pp collisions at 13 TeV with the ATLAS detector. ATLAS-CONF-2023-019, 2023. URL `https://cds.cern.ch/record/2855337`.

[8] ATLAS Collaboration. Inclusive and differential cross section measurements of $t\bar{t}Z$ production in pp collisions at $\sqrt{s} = 13$ TeV with the ATLAS detector, including EFT and spin correlations interpretations. ATLAS-CONF-2023-065, 2023. URL `https://cds.cern.ch/record/2873519`.

[9] ATLAS Collaboration. Measurement of jet substructure in boosted $t\bar{t}$ events with the ATLAS detector using 140 fb^{-1} of 13 TeV pp collisions. ATLAS-CONF-2023-027, 2023. URL `https://cds.cern.ch/record/2861056`.

[10] ATLAS Collaboration. Observation of four-top-quark production in the multilepton final state with the ATLAS detector. *Eur. Phys. J. C*, 83: 496, 2023. doi: 10.1140/epjc/s10052-023-11573-0.

[11] ATLAS Collaboration. Observation of $t\bar{t}$ production in lepton+jets and dilepton channels in p+Pb collisions at $\sqrt{s_{\mathrm{NN}}} = 8.16$ TeV with the ATLAS detector. ATLAS-CONF-2023-063, 2023. URL `https://cds.cern.ch/record/2873517`.

[12] ATLAS and CMS Collaborations. Combination of measurements of the top quark mass from data collected by the ATLAS and CMS experiments at $\sqrt{s} = 7$ and 8 TeV. ATLAS-CONF-2023-066, 2023. URL `https://cds.cern.ch/record/2873520`.

[13] ATLAS Collaboration. Observation of quantum entanglement in top-quark pairs using the ATLAS detector. *arXiv: 2311.07288 [hep-ex]*, 2023.

[14] ATLAS Collaboration. Search for flavor-changing neutral tqH interactions with $H \to \gamma\gamma$ in pp collisions at $\sqrt{s} = 13$ TeV using the ATLAS detector. *arXiv: 2309.12817 [hep-ex]*, 2023.

[15] Louis Lyons, Duncan Gibaut, and Peter Clifford. How to combine correlated estimates of a single physical quantity. *Nuclear Instruments and Methods in Physics Research Section A: Accelerators, Spectrometers, Detectors and Associated Equipment*, 270(1):110–117, 1988. ISSN 0168-9002. doi: https://doi.org/10.1016/0168-9002(88)90018-6.